RSC Advances

PAPER

View Article Online
View Journal | View Issue

Cite this: *RSC Adv.*, 2020, **10**, 15000

Antibacterial activity evaluation and mode of action study of novel thiazole-quinolinium derivatives†

Ying Li,‡[a] Ning Sun, ‡*[abc] Hooi-Leng Ser,[ad] Wei Long,[a] Yanan Li,[e] Cuicui Chen,[a] Boxin Zheng,[a] Xuanhe Huang,[a] Zhihua Liu*[b] and Yu-Jing Lu*[a]

New antimicrobial agents are urgently needed to address the emergence of multi-drug resistant organisms, especially those active compounds with new mechanisms of action. Based on the molecular structures of the FtsZ inhibitors reported, a variety of thiazole-quinolinium derivatives with aliphatic amino and/or styrene substituents were synthesized from benzothiazolidine derivatives. In the present study, to further explore the antibacterial potential of thiazole-quinolinium derivatives, several Gram-positive and Gram-negative bacteria were treated with the newly modified compounds and the biological effects were studied in detail in order to understand the bactericidal action of the compounds. Our findings reveal that some of these derivatives possess good potent bactericidal activity as they can inhibit Gram-positive methicillin-resistant *Staphylococcus aureus*, vancomycin-resistant *Enterococcus* and also some Gram-negative organisms and NDM-1 *Escherichia coli*. Furthermore, compounds **4a1–4a4** and **4b1–4b4** altered the morphology of bacterial cells and the cells displayed a more-elongated shape compared to the untreated cells. Biochemical assays showed that **4a4** and **4b4** stimulate FtsZ polymerization in bacterial cells, which eventually disrupts its dynamic assembly and Z-ring formation. The inhibition of this crucial step in bacterial cell division could potentially represent their main mechanism of antibacterial activity. Cytotoxicity assay and hemolysis assay suggested that **4a4** and **4b4** possess low cytotoxicity. In summary, these results further highlight the importance of **4a4** and **4b4** that could be developed as potent and effective bacteriostatic agents against multi-drug resistant bacteria.

Received 22nd January 2020
Accepted 7th April 2020

DOI: 10.1039/d0ra00691b

rsc.li/rsc-advances

1. Introduction

Since the discovery of penicillin in the 1930s, antibiotics have been the most common choice and effective practice to treat bacterial infection and related diseases. Even so, the overuse and mismanagement of antibiotics have resulted in the anti-microbial resistance crisis. For instance, methicillin-resistant *Staphylococcus aureus* (MRSA), vancomycin-resistant *Enterococcus* (VRE) and NDM-1 *Escherichia coli* pose great threat to human health as these strains are resistant to most of the conventional antibiotics. In fact, most of them carry antibiotic resistance genes that make them survive against antibiotics (*e.g.* enzymatic degradation).[1,2] Nowadays, the emergence of "superbugs" is considered as one of the greatest scientific challenges worldwide and urges the discovery of new antibacterial agents with novel mechanisms of actions.[3–5]

One of the classical target pathways for antibacterial agents is cell division process.[6] Bacterial cell division is mediated by a highly dynamic, large protein complex divisome, which involves a time-dependent assembly of specific cell division proteins. Divisome formation is orchestrated by the essential tubulin homolog FtsZ (filamenting temperature sensitive mutant).[7] At the initiation of cell division, FtsZ migrates to the division site and assembles into protofilaments in a GTP dependent manner. After that, a ring-like structure, which was called the Z-ring, forms at the prospective division site. Towards the end of the cell division process, Z-ring constricts to induce septum formation before the completion of cell division.[8] FtsZ shows high conservation, structural similarity and functional importance among bacteria and thus it presents as one of the imperative targets for the development of new antibiotic agents.

[a]*School of Biomedical and Pharmaceutical Sciences, Guangdong University of Technology, Guangzhou 510006, PR China. E-mail: luyj@gdut.edu.cn*

[b]*The State Key Laboratory of Chemical Biology and Drug Discovery, Department of Applied Biology and Chemical Technology, The Hong Kong Polytechnic University, Hung Hom, Kowloon, Hong Kong, China. E-mail: ning.sun@connect.polyu.hk; liuzhihualzh@hotmail.com*

[c]*The Fifth Affiliated Hospital of Guangzhou Medical University, Guangzhou 510700, PR China*

[d]*Novel Bacteria and Drug Discovery (NBDD) Research Group, Microbiome and Bioresource Research Strength, Jeffrey Cheah School of Medicine and Health Sciences, Monash University Malaysia, 47500 Bandar Sunway, Selangor Darul Ehsan, Malaysia*

[e]*Department of Pharmacy, The Fifth Affiliated Hospital of Sun Yat-sen University, Zhuhai, 519000, P. R. China*

† Electronic supplementary information (ESI) available. See DOI: 10.1039/d0ra00691b

‡ These authors contributed equally to this work.

In recent years, some compounds with inhibitory action on bacterial cell division are potential candidates to be developed as new antibiotics and they have also gained much attention from the scientific community and drug companies.[8] FtsZ inhibitors are capable of disturbing the dynamic polymerization of FtsZ and Z-ring formation, which ultimately impede bacterial cell division.[6,9–12] Among the known FtsZ inhibitors, taxane derivative[7] and SRI-3072 (ref. 13) were known to inhibit FtsZ polymerization effectively, particularly against drug-resistant *Mycobacterium tuberculosis*. Besides, Zantrins inhibited GTPase activity of FtsZ and perturbed cytokinetic ring assembly.[6] PC190723 displayed potent bactericidal activity with good selectivity against *Staphylococci*, as shown in the *in vitro* screening assay using multi-drug resistant *Staphylococcus aureus* and a rodent model with MRSA infection.[11] Recently, we have reported some FtsZ inhibitors with good antibacterial activity including berberine derivatives,[14] tiplaxtinin,[15] and quinolinium derivative.[4] In addition, some macrolide derivatives containing quinoline or benzothiazole scaffolds,[16] quinoline and quinolone derivatives[17] were found exhibiting good antibacterial effects. We analyzed the molecular structures of these active compounds and found that the scaffold of benzothiazole or quinoline is generally effective in preventing bacterial cell division by interrupting the normal function of FtsZ protein. Our recent study targeting FtsZ inhibition by applying thiazole orange[4] and benzofuroquinolinium derivatives[18] (Fig. 1) prompted us to further investigate the antibacterial activity and mode of action for a combined scaffold of thiazole-quinolinium. In the present study, we synthesized **17** new thiazole-quinolinium derivatives (Table 1) and conducted a series of bioassays to investigate their antibacterial ability and elucidate the possible mode of action.

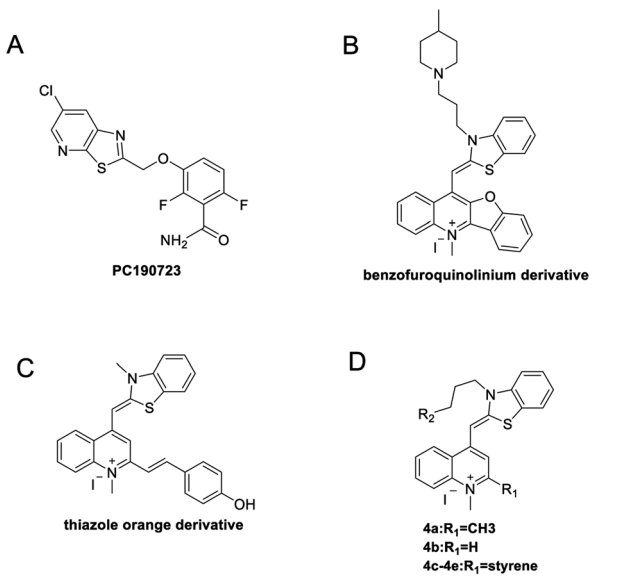

Fig. 1 Chemical structures of PC190723 (A), benzofuroquinolinium derivative (B), thiazole orange derivative (C), and thiazole-quinolinium derivatives **4a–4e** (D).

Table 1 Chemical structures of the target thiazole-quinolinium derivatives

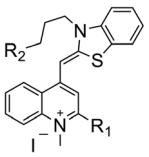

Compound	R_1	R_2
4a1	CH_3	
4a2		
4a3		
4a4		
4b1	H	
4b2		
4b3		
4b4		
4c1	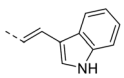	
4c2	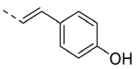	
4d1	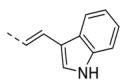	
4d2	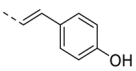	
4d3	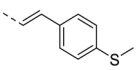	
4e1	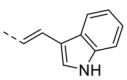	
4e2	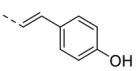	
4e3	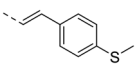	
4e4	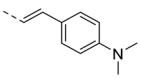	

2. Results and discussion

2.1. Design and synthesis of the thiazole-quinolinium derivatives

Our results showed that some molecules contain benzothiazole or quinoline scaffold may have good antibacterial activity by

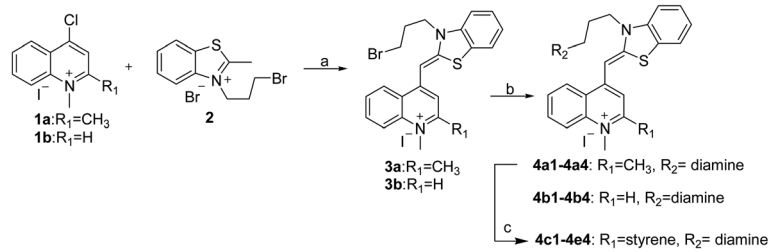

Scheme 1 Synthetic route of thiazole-quinolinium derivatives. Reagents and conditions: (a) methanol, sodium bicarbonate, 45 °C, 3 h; (b) reaction with different diamines, potassium iodide, 45 °C, 24 h; (c) reaction with different aromatic aldehydes, 130 °C, 3 h.

interrupting the function of FtsZ protein.[4,19] Thiazole orange derivative (Fig. 1C) possesses strong bacterial cell growth inhibitory effect. This compound enhances FtsZ polymerization *in vitro*. The prediction model also showed that it binds to the interdomain cleft delimited by H7-helix and T7-loop of FtsZ.[4] Benzofuroquinolinium derivative[18] (Fig. 1B) has also been demonstrated targeting FtsZ and showing good antibacterial activity. We therefore retained the benzothiazolidine or quinone core for designing new antibacterial compounds. In the present study, we introduced a fatty amino substituent at 3-position of benzothiazole of the compound. In addition, a styrene substituent was introduced at 2-position of quinoline in compounds **4c1–4e4**. The antibacterial activity and mode of action were used to investigate whether these new thiazole-quinolinium compounds possess antibacterial activity targeting FtsZ.

The new thiazole-quinolinium derivatives (**4a–e**) shown in Table 1 were prepared in good yields by following the reported procedures[20,21] (Scheme 1). Intermediates **3a** and **3b** were obtained by the reaction of 1,2-dimethyl-4-chloroquinolinium iodide or *N*-methyl-4-chloroquinolinium with *N*-(3-bromopropyl)-2-methylbenzo[*d*]thiazolium iodide in the presence of sodium bicarbonate. The reaction of **3a** or **3b** with a secondary amine including morpholine, diethylamine, piperidine and pyrrolidine afforded compounds **4a** and **4b** in good yields. Further reaction of **4a** or **4b** with different aromatic aldehydes including 4-hydroxybenzaldehyde, 4-(methylthio)benzaldehyde, 4-(dimethylamino)benzaldehyde, and indole-2-carboxaldehyde to afford the targeted compounds **4c–e**. All the compounds were purified by flash silica gel column chromatography and were confirmed with ^{1}H NMR, ^{13}C NMR, ESI-MS or HRMS (Fig. S11–S24†). The synthesis of intermediates **1a**, **1b** and **2** was followed the reported methods.[21] Compounds **4a2**, **4b1** and **4b2** were reported as the fluorescent bio-molecular sensors.[21]

2.2. Antibacterial activity of the thiazole-quinolinium derivatives

The antimicrobial test showed that these thiazole-quinolinium derivatives possess broad-spectrum, potent antibacterial activity against a majority of selected Gram-positive and some Gram-negative strains, including four MRSA strains and drug resistant *E. coli* strain as shown in Tables 2 and 3. In general, all compounds reduced significantly the growth of antibiotic-susceptible and antibiotic-resistant *S. aureus* strains with MIC values in a range of 1–32 μg mL^{-1}. Some analogues against MRSA strains were found 100 times more potent than methicillin. In addition, *S. epidermidis* was inhibited by the compounds with MIC values ranged from 0.25 to 16 μg mL^{-1}. These thiazole-quinolinium derivatives were able to inhibit the growth of vancomycin-resistant *E. faecium* with MIC values of 2–32 μg mL^{-1} and also indicated that these compounds were much more effective than vancomycin. Interestingly, while all positive controls used in the study including methicillin, vancomycin, ampicillin and rifampin were not able to reduce the growth of the antibiotics resistant *E. coli* mutant NDM-1 strain (MIC > 64 μg mL^{-1}), the new compounds inhibited both antibiotic susceptible strain and NDM-1 strain with MIC values of 0.5–64 μg mL^{-1}.

By analyzing the MIC results obtained from the antimicrobial screening with respect to the molecular structure of the compounds, the antibacterial activity was found obviously influenced by the two substituent groups, R_1 on the quinoline fragment and R_2 on the benzothiazole fragment. It seems that R_1 group gives a more determining effect on the antibacterial activity. We found that the size of the R_1 group was also critical, in which CH_3 group was the best as it is larger than H and is much less bulky than *p*-substituted styryl group and indolyl group. The effect of R_1 group in antibacterial activity may roughly show in the following order: CH_3 > H ≫ indolyl ≈ styryl. This observation may also suggest that the binding pocket of the FtsZ protein was steric sensitivity. For R_2 group substituted *N*-benzothiazole fragments, there were five amino groups including diethyl amine, pyrrolidine, piperidine, 4-methylpiperidine, and morpholine, which were attached to *N*-benzothiazole moiety through an ethyl bridge. When R_1 group was either CH_3 or H, both diethyl amine and 4-methylpiperidine gave the best antibacterial activity, whereas pyrrolidine and piperidine gave much less inhibitory potency. When R_1 was a bulky group, the substituent of R_2 seems no significant influence on the inhibitory potency. However, for the compounds with the substituent R_1 was an indolyl (**4c1**, **4d1**, **4e1**), the pyrrolidine substituent gave slightly better antibacterial activity than other analogues. In general, the antibacterial results indicated that the amino terminal group of benzothiazole fragment and a small group substituted at the quinoline 2-position were essential in conferring the potent antibacterial activity of the thiazole-quinolinium derivatives.

Table 2 MICs of the synthesized compounds against Gram-positive bacteria strains (μg mL^{-1})

	Bacterial strains										
	S. aureus ATCC 29213	*S. aureus* ATCC 43300[a]	*S. aureus* ATCC BAA-41[a]	*S. aureus* ATCC BAA-44	*S. aureus* ATCC BAA-1747[a]	*S. aureus* ATCC BAA-1720[a]	*E. faecalis* ATCC 29212	*E. faecium* ATCC 49624	*E. faecium* ATCC 700221[b]	*S. epidermidis* ATCC 12228	*B. subtilis* 168
4a1	2	4	2	4	8	8	32	16	16	1	8
4a2	32	32	8	8	32	32	64	32	32	4	8
4a3	32	32	8	8	32	32	64	32	32	8	8
4a4	1	2	1	1	2	2	2	1	2	0.5	1
4b1	2	8	2	2	16	16	32	8	2	1	8
4b2	32	8	4	4	16	16	32	16	32	4	8
4b3	32	8	4	4	8	16	>64	32	32	2	16
4b4	2	8	1	2	4	8	16	8	16	0.25	4
4c1	16	16	16	8	16	16	16	16	8	2	8
4c2	16	16	8	8	16	32	16	8	4	4	4
4d1	16	8	4	4	8	8	32	8	16	2	2
4d2	32	32	32	32	32	32	64	32	32	16	16
4d3	16	32	32	32	32	32	64	64	32	16	16
4e1	16	16	16	16	32	16	>64	32	8	16	8
4e2	16	8	16	16	32	16	>64	16	8	8	4
4e3	8	8	16	8	16	16	>64	16	8	4	8
4e4	16	8	16	8	16	8	32	32	4	2	8
amp[c]	>64	>64	>64	16	>64	>64	0.5	0.25	>64	>64	32
van[c]	2	2	2	1	1	0.5	2	0.5	1024	>64	0.25
meth[c]	0.5	512	1024	1024	256	1024	1	4	1.5	0.5	0.625
rif[c]	0.5	<0.125	<0.125	2	<0.125	<0.125	0.5	<0.125	<0.125	1	4

[a] These strains are MRSA. [b] Vancomycin-resistant strain, MIC of vancomycin is 1024 μg mL^{-1}. [c] amp: ampicillin; van: vancomycin; meth: methicillin; rif: rifampin.

Table 3 MICs of the synthesized compounds against Gram-negative bacteria strains (μg mL^{-1})

	Bacterial strains						
	E. coli ATCC 25922	*E. coli* ATCC 8739	*E. coli* ATCC BAA-2469[a]	*K. pneumoniae* ATCC BAA-2470[a]	*A. baumannii* ATCC 19606[b]	*P. aeruginosa* ATCC BAA-2108[b]	*E. cloacae* ATCC BAA-1143[c]
4a1	2	4	8	32	64	64	>64
4a2	4	8	4	64	64	64	64
4a3	4	4	4	32	64	64	>64
4a4	0.5	1	1	8	16	64	64
4b1	2	8	1	32	64	64	>64
4b2	4	4	2	32	64	64	>64
4b3	2	4	4	32	64	64	>64
4b4	2	2	0.5	8	16	16	>64
4c1	8	64	64	>64	>64	>64	>64
4c2	4	32	8	>64	>64	>64	>64
4d1	4	16	4	16	32	32	64
4d2	32	32	16	>64	>64	>64	>64
4d3	16	32	32	64	64	64	>64
4e1	16	32	16	64	>64	>64	>64
4e2	4	16	8	64	>64	64	>64
4e3	16	32	16	64	64	32	64
4e4	16	16	8	32	>64	64	64
amp[d]	1	2	>64	>64	64	>64	>64
van[d]	>64	>64	>64	>64	64	>64	>64
meth[d]	2	>64	>2048	>2048	>256	>64	>96
rif[d]	4	8	>64	>64	1	>64	64

[a] NDM-1 expressing strain, which is resistant to most of the antibiotics, except tigecycline and colistin. [b] Multi-drug resistant strain. [c] AmpC beta-lactamase expressing strain. [d] amp: ampicillin; van: vancomycin; meth: methicillin; rif: rifampin.

In the present study, we screened out four compounds (**4a1**, **4a4**, **4b1**, **4b4**) that showed greater antibacterial activity than their analogues (Tables 2 and 3). For example, **4a4** inhibited the growth of antibiotic-susceptible and antibiotic-resistant *S. aureus* strains with MIC values in a very low range of 1–2 μg mL^{-1}. The antibacterial activity of **4a4** against MRSA strains was lower than rifampin but comparable to that of vancomycin. In addition, the growth of *E. faecium*, *S. epidermidis* and *E. coli* could be inhibited by **4a4** with MIC values of 0.5–2 μg mL^{-1}. Moreover, **4a4** also displayed moderate antibacterial activity against drug-resistant *K. pneumoniae*, *A. baumannii*, *P. aeruginosa* and *E. cloacae*, which were resistant to most of the positive controls of commonly prescribed antibacterial agents such as methicillin, vancomycin and ampicillin (Tables 2 and 3).

In order to further investigate the antibacterial activity of these compounds, we evaluated the minimum bactericidal concentrations (MBCs) of four selected compounds (**4a1**, **4a4**, **4b1** and **4b4**) against *S. aureus* ATCC 29213 and *E. faecium* ATCC 700221. The MBC values were summarized in Table 4. As indicated by the MBC/MIC ratio > 4, the results suggested that the compounds may exert bacteriostatic action (Table 5).[22,23]

Table 4 MBCs of selected compounds against two bacteria strains (μg mL^{-1})

	MBC (μg mL^{-1})	MIC (μg mL^{-1})	MBC/MIC
***E. faecium* ATCC 700221**			
4a1	128	16	8
4a4	>64	2	>32
4b1	16	2	8
4b4	128	16	8
***S. aureus* ATCC 29213**			
4a1	64	2	32
4a4	8	1	8
4b1	32	2	16
4b4	16	2	8

2.3. Thiazole-quinolinium derivatives inhibited bacterial cell division

FtsZ inhibitors can effectively inhibit bacterial cell division, which triggers the elongation of *B. subtilis* cells.[11] We therefore visualized the cell morphology of *B. subtilis* incubated with or without the thiazole-quinolinium derivatives. The results showed that the compounds bearing a small group, either H or

Table 5 Cytotoxicity results of compounds 4a4 and 4b4

	S. aureus ATCC 29213 (MIC, μg mL^{-1})		IC_{50}, μg mL^{-1}	
	4a4	**4b4**	**4a4**	**4b4**
16HBE	1	2	14.3	20.2
HK-2	1	2	26.0	18.6
L929	1	2	12.6	23.4

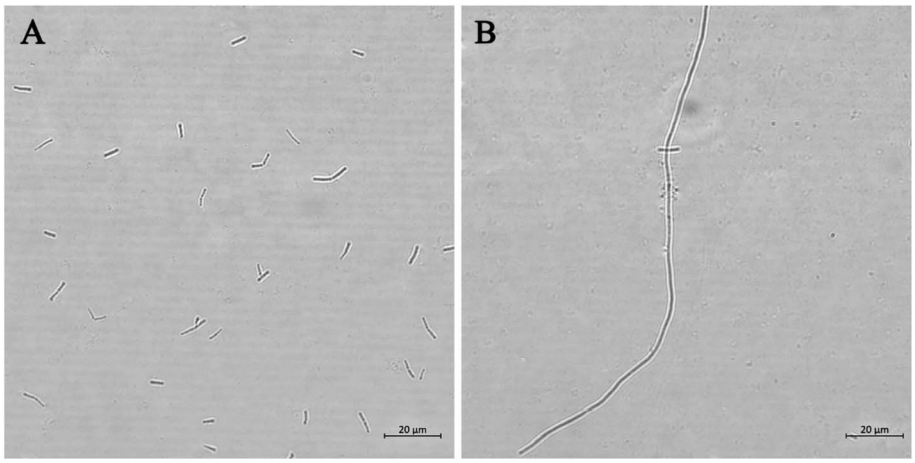

Fig. 2 Morphology analysis of *B. subtilis* 168. Cells were grown in the absence (A) and presence of **4a4** (B). Scale bar = 20 μm.

CH_3, at the 2-position of quinoline, such as **4a1–4a4** and **4b1–4b4**, were able to induce bacterial cells elongation (Fig. 2 and S1†). For example, the cell length of *B. subtilis* 168 in the control group was 5–10 μm, whereas after incubation with **4a4** at 0.5 μg mL^{-1} for 4 h, the bacteria were found longer than 10 μm, suggesting a mechanism of antibacterial-induced cell filamentation. However, for other compounds, including all analogues from **4c**, **4d**, and **4e** series, bearing a bulky substituent group (strylyl or indolyl moiety) at the 2-position of quinoline, they only exhibited very little effect on bacterial cell elongation. These results suggested that the addition of bulky substitute group at 2-position of quinoline core may cause significant reduction in cell division targetability and antibacterial activity.

2.4. Thiazole-quinolinium derivatives disrupted FtsZ function *in vitro*

Some inhibitors such as PC190723 (ref. 11) and berberine[10] induce cell filamentation by interacting with FtsZ protein. The cell elongation-induced by our compounds may be also *via* the interactions with FtsZ protein. In order to elucidate the mechanism of antibacterial activity, dynamic polymerization of FtsZ by light scattering test was studied using two groups of selected compounds: (a) compounds **4a4** and **4b4** induced elongation of the bacteria; (b) compounds **4e1** and **4e3** did not promote elongation of bacteria. First, the light scattering signals of **4a4**, **4b4**, **4e1** and **4e3** with the same concentration were measured under the same test conditions (Fig. 3A). It was found that **4a4** and **4b4** caused a significant increase in light scattering signal compared to the control signal. On the contrary, **4e1** and **4e3** caused almost no signal change. We then further measured the light scattering signals of **4a4**, **4b4**, **4e1** and **4e3** at a certain concentration gradient. The results showed that **4a4** and **4b4** could enhance FtsZ polymerization in a dose-dependent manner (Fig. 3B and S4†). Similar enhancement effect on polymerization of FtsZ protein could also be observed in some of the FtsZ-targeting compounds, such as thiazole orange derivative (Fig. 1C),[4] PC190723 (Fig. 1A)[24] and its analogs.[25] However, under the same conditions, the light scattering signals of **4e1** and **4e3** did not show significant change (Fig. S4†). These results therefore revealed that the compounds with H or CH_3 group at 2-position of quinoline core (**4a4** and **4b4**) had a stronger stimulation effect on FtsZ polymerization

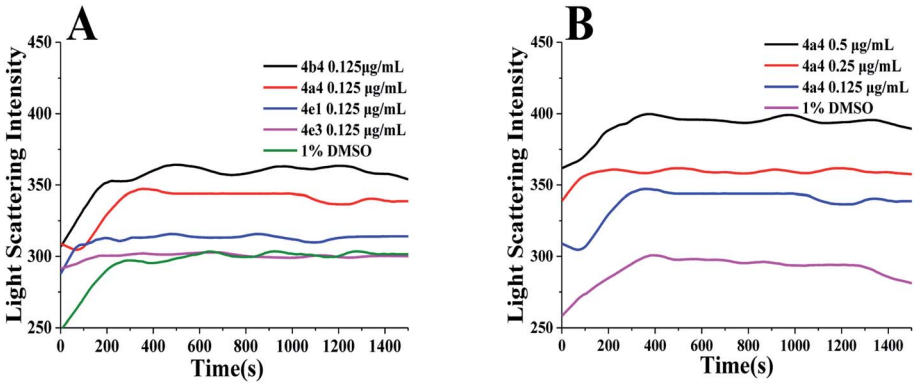

Fig. 3 (A) Effect of compounds **4a4**, **4b4**, **4e3** and **4e1** on the polymerization of FtsZ at a concentration of 0.125 μg mL^{-1}. (B) Effect of **4a4** on the polymerization of FtsZ at a concentration of 0.125–0.5 μg mL^{-1}.

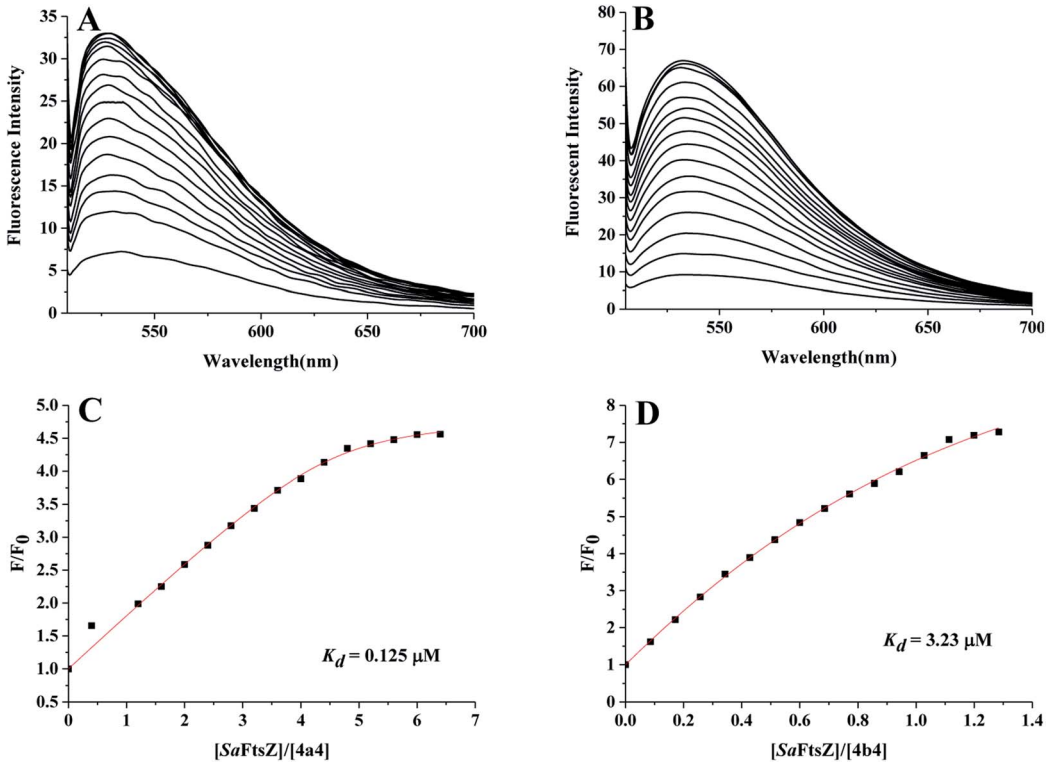

Fig. 4 (A and B) Fluorescence titration spectra of 3.51 μM **4a4** (A) and 3.68 μM **4b4** (B) in the absence and presence of *Sa*FtsZ at concentrations ranging from 0.4 to 6.4 μM. (C and D) Nonlinear fit diagram of the binding constants of compounds **4a4** (C) and **4b4** (D).

than those with bulky groups (**4e1** and **4e3**). This indicated that the small-sized substituent at 2-position of quinoline core plays a pivotal role in the inhibitor–FtsZ interaction. Conversely, the bulky substituent group may hamper compound–FtsZ interaction that renders these compounds fail to target FtsZ and lose inhibitory ability to cell division.

The dynamic assembly of FtsZ was strictly regulated by its GTPase activity,[11,26] the GTPase activity of *S. aureus* FtsZ (*Sa*FtsZ) was determined using a ATPase/GTPase Activity Assay Kit (Sigma-Aldrich, USA) according to the manufacturer's instructions with minor modifications.[27] The results showed that **4a4** and **4b4** did not show any effect on the GTPase activity of *Sa*FtsZ (Fig. S5†).

2.5. Binding study of the compounds with *Sa*FtsZ

To further determine the ability of a thiazoquinoline derivative to target *Sa*FtsZ. We selected two compounds **4a4** and **4b4** with good antibacterial activity and monitored the intrinsic

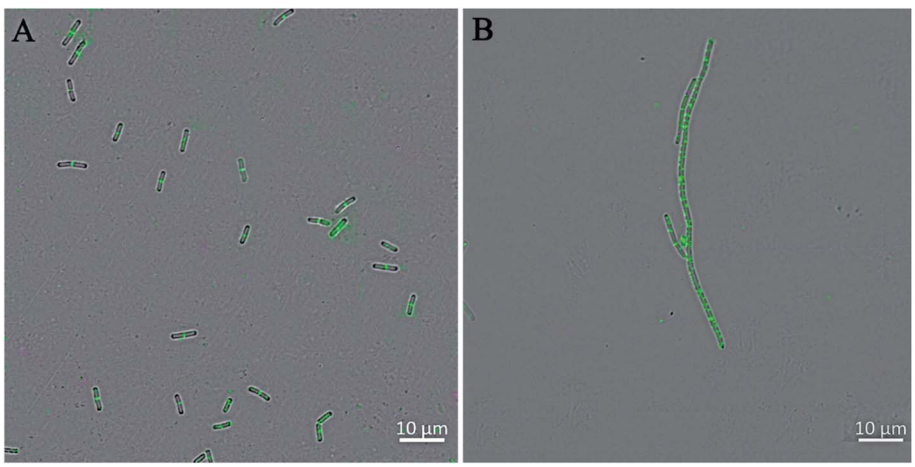

Fig. 5 The perturbation of the cytokinetic Z-ring in *B. subtilis*. Cells of *B. subtilis* were grown in the absence (A) and presence of **4a4** (B). Scale bar = 10 μm.

fluorescence of the compound with the addition of *Sa*FtsZ. From Fig. 4A and B, when increasing the *Sa*FtsZ concentration, the fluorescence intensity of both compounds was enhanced remarkably. The FtsZ-induced fluorescence indicated the compound bound to *Sa*FtsZ. We therefore determined the FtsZ-compound dissociation constant (K_d) of the binding reaction according to the independent site model[28] by nonlinear fitting to the equation:[29] $F/F_0 = 1 + (Q - 1)/2\ (N + 1 + X - ((X + 1 + N)^2 4X)^{1/2})$. In this relationship, F_0 and F are the fluorescence emission intensities of the compound in the absence and presence of protein, respectively; $N = (K_a C_{compound})^{-1}$, $Q = F_{max}(F_0)^{-1}$, $X = nC_{SaFtsZ}(C_{compound})^{-1}$, $K_a = K_d{}^{-1}$, F_{max} is the fluorescence intensity upon saturation of *Sa*FtsZ.

From Fig. 4C and D, the K_d values of **4a4** and **4b4** were 0.125 μM and 3.23 μM, respectively, by comparing the dissociation constants estimated, **4a4** with a CH_3 group at 2-position of quinoline fragment had a greater affinity for *Sa*FtsZ than **4b4**. This may indicated that the CH_3 group is more likely to enhance the binding affinity of the compound.

2.6. Effects of the synthesized compounds on *B. subtilis* Z-ring formation in *B. subtilis*

The perturbation of the Z-ring can also pre-maturely inhibit the bacterial cell division and induce bacterial cell elongation.[10,30,31] Therefore, four compounds with strong antibacterial activity and cell inhibitory effects, **4a1**, **4a4**, **4b1** and **4b4**, were used to treat *B. subtilis* before determining their effects on Z-ring formation (Fig. 5 and S6†). In the absence of compounds, a bright green fluorescent band at the cell midpoint was apparently observed, representing the septation–competent localized Z-rings (cytoskeletal structures) (Fig. 5A). Comparatively, GFP-FtsZ dispensed as discrete foci throughout the elongated cell after the treatment with **4a1**, **4a4**, **4b1** or **4b4** (Fig. 5B and S6†), suggesting that these compounds promoted the mislocalization of the FtsZ protein.

2.7. Cytotoxicity of selected synthesized compounds

Cytotoxicity of two representative thiazole-quinolinium derivatives, **4a4** and **4b4**, with best antibacterial activity was examined against human bronchial epithelium cells (16HBE), human renal tubular epithelial cells (HK-2), and mouse fibroblast cells (L929). The IC_{50} values of **4b4** for the 16HBE and L929 cell lines were greater than **4a4**, whereas the IC_{50} values of **4b4** were less than **4a4** for the HK-2 cell line. For these three cell lines, the IC_{50} values of **4a4** and **4b4** were much greater than MIC values of these compounds against *S. aureus* ATCC 29213, which indicated that **4a4** and **4b4** may not have significant cytotoxicity against normal human cells. In addition, hemolytic activity test[32] was also used to detect the toxicity of **4a4** and **4b4**. The result showed that **4a4** and **4b4** did not exhibit hemolytic toxicity to human erythrocytes (Fig. S7†).

2.8. *In vitro* evaluation of potential resistance development

In order to evaluate the potential development of drug resistance of **4a4** and **4b4**, three commercial antibiotics (ciprofloxacin, vancomycin and rifampin) were used as positive controls against *S. aureus* ATCC 29213. As shown in Fig. 6, the MIC values of **4a4** and **4b4** against *S. aureus* ATCC 29213 only increased by 16-fold and 8-fold, respectively, after 35 passages. Comparatively, the MIC values of ciprofloxacin, vancomycin and rifampin increased 32-fold, 512-fold and 8192-fold, respectively. Similar results were obtained when these compounds were used to treat *B. subtilis* 168 and *E. coli* ATCC 25922 (Fig. S8 and S9†). Based on the results of drug resistance study, **4a4** and **4b4** produced low forced induction of resistance on the tested strains.

2.9. Predicted binding mode of 4a4 to FtsZ

The biological assay results indicated that **4a4–4b4** may potentially be effective FtsZ targeting inhibitors. Molecular modeling studies were performed to detect potential binding sites of **4a4** and **4b4** to FtsZ protein. One relatively inactive compound **4e1** was also performed in this test for comparison. As a result, the highest docking score for **4a4** and **4b4** binding were obtained near the T7-loop and the H7-helix, and the binding site was a relatively narrow interdomain cleft defined by H7-helix, T7-loop and quadruplex β-sheets (Fig. 7A and S10A†). The whole structure of **4a4** (Fig. S10A,† green) and **4b4**

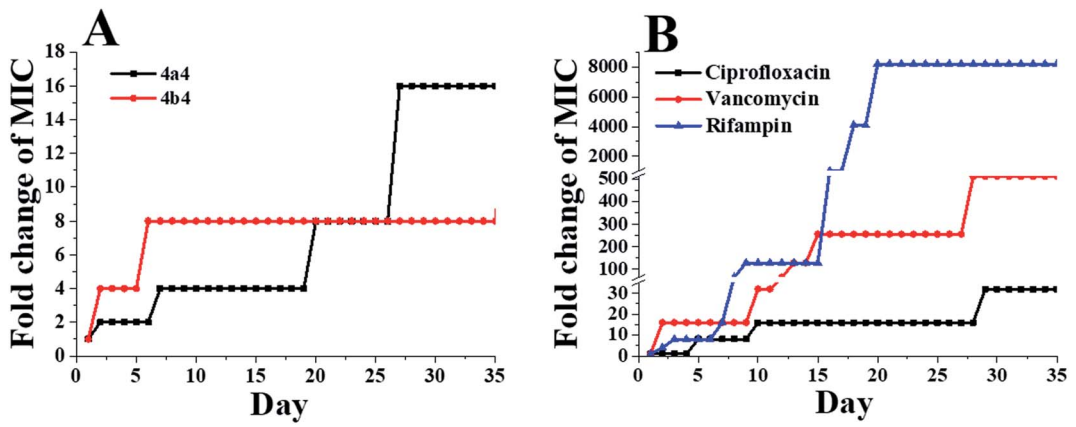

Fig. 6 Bacterial resistance study of selected compounds against *S. aureus* ATCC 29213: **4a4** and **4b4** (A) and ciprofloxacin, vancomycin and rifampin (B).

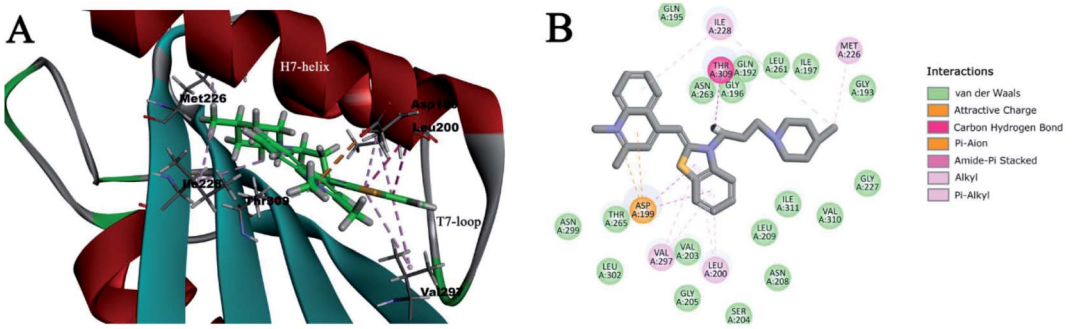

Fig. 7 (A) Molecular modeling studies of **4a4** with FtsZ protein. This compound was predicted to bind into the C-terminal interdomain cleft of FtsZ; (B) predicted interactions between **4a4** and the amino acids of FtsZ.

(Fig. S10A,† yellow) was found to locate in the cleft. On the other hand, only part of **4e1** binded into the binding site (Fig. S10A,† purple). A 2D diagram (Fig. 7B) showed the predicted interactions between **4a4** and FtsZ residues. It was predicted that a large number of hydrophobic interactions between **4a4** and Asp 199, Ile228, Met226, Val297 and Leu200 of FtsZ protein. In addition, electrostatic interactions and hydrophobic interactions could be found between benzothiazolidine and Asp199. A carbon–hydrogen bond was discovered between the fatty ammonia carbon chain and Thr309. Furthermore, in the binding pocket, a large number of amino acid residues such as Gln195, Val310, Gly205, Ile311 may have interactions with **4a4** *via* van der Waals forces. The predicted interactions between **4b4** and FtsZ were similar to that of **4a4**. However, as shown in Fig. S10B,† Thr309 and Ile311 cannot establish interaction with **4b4**, and this maybe the reason that **4a4** with a CH_3 group at 2-position of quinoline fragment had a greater affinity for *Sa*FtsZ than **4b4**. In contrast, fewer interactions between **4e1** and FtsZ were predicted (Fig. S10C†) when compared with those of **4a4** and **4b4**. For instance, it was found that **4e1** showed a charge attraction with Asp199 only.

3. Discussion and conclusions

In summary, a series of new thiazole-quinolinium derivatives were synthesized and their antibacterial activity and possible mode of action were thoroughly investigated. Antimicrobial susceptibility test confirmed that these thiazole-quinolinium derivatives possess broad-spectrum antibacterial activity against Gram-positive and Gram-negative strains, including some highly resistant strains. Among the compounds tested, **4a4** and **4b4** bearing a small group (CH_3 or H) at 2-position of quinoline fragment exhibited potent antibacterial activity against MRSA and VRE and low MIC values at 1–8 μg mL^{-1} and 2–16 μg mL^{-1} were obtained. The inhibitory effects were comparable to the reported FtsZ inhibitors. 9-Phenoxyalkylberberine derivative **2** inhibited the cell proliferation with MIC values from 2 to 8 μg mL^{-1} against MRSA and VRE.[14] A benzamide prodrug of PC190723 (TXA709) inhibited the cell division with MIC values from 2 to 4 μg mL^{-1} against MRSA.[12] PC190723 inhibited the proliferation of *S. aureus* strains at 1 μg mL^{-1}.[33] In addition, **4a4** and **4b4** inhibited the growth of *E. coli* and its antibiotics resistant mutant with MIC values of 0.5–2 μg mL^{-1}. To date, a few FtsZ inhibitors have been reported with strong antibacterial activity against Gram-negative bacteria. For example, 9-phenoxyalkylberberine derivative **2** inhibited the growth of *E. coli* with MIC value of 32 μg mL^{-1}.[14] Thiazole orange derivative **1** (Fig. 1C) has MIC values from 0.75 to 48 μg mL^{-1} against the Gram-negative strains.[4] The antibacterial activity of **4a4** and **4b4** against Gram-negative bacteria may be attributed to the ability of the compound to pass through the outer membrane of Gram-negative bacteria. In the morphological study, both compounds significantly increased the cell length of *B. subtilis* 168 by inhibiting Z-ring formation, without interfering with its membrane integrity, suggesting that compounds interact with Z-ring to inhibit bacterial cytokinesis. **4a4** and **4b4** were also found to bind to FtsZ and thus to promote FtsZ polymerization in a dose-dependent manner without interfering GTPase activity. Similar enhancement effect on polymerization of FtsZ protein could also be observed in some of FtsZ-targeting compounds, such as thiazole orange derivative (Fig. 1C),[4] PC190723 (Fig. 1A)[24] and its analogs.[25] The phenomenon that the compounds did not significantly affect the GTPase activity of *Sa*FtsZ also appears in some reported FtsZ inhibitors, such as 2,6-difluoro-3-aminobenzamide derivative[34] and the derivatives of PC190723,[35] which were reported to bind to the interdomain cleft of FtsZ. Moreover, both cytotoxic and hemolysis experiments indicated that **4a4** and **4b4** showed no significant cytotoxicity to normal cells. Drug resistance experiments also showed that **4a4** and **4b4** were not easy to induce bacterial resistance. Based on these results obtained, **4a4** and **4b4** may be good candidates for the development of new antibacterial agents targeting drug-resistant bacteria.

4. Materials and methods

4.1. Chemistry

All analytical grade reagents and chemicals were used as received without further purification and purchased from Aladdin and Sigma. Mass spectra (MS) were recorded on Bruker amazon SL mass spectrometer with an ESI or ACPI mass selective detector and the high-resolution mass spectra (HRMS) were recorded with Agilent 12606230TOF. ^1H and ^{13}C NMR spectra were recorded in DMSO using TMS as the reference with

a Bruker BioSpin GmbH spectrometer at 400 MHz and 100 MHz, respectively. Elemental analyses were carried out on an Elementar Vario EL CHNS elemental analyzer.

4.2. General synthetic procedure for the intermediates (1a–1b, 2a and 3a–3b)

Intermediates **1a** and **1b** was obtained by the reaction of 4-chloro-2-methylquinoline (2 g, 11.24 mmol) or 4-chloroquinoline (2 g, 12.27 mmol) with iodomethane (9.6 g) in tetramethylene sulfone (4.5 mL). After stirring at 65 °C for 24 h the reaction mixed was cooled and suction filtration was performed before the addition of ethyl acetate. The solid was washed again with ethyl acetate and dried in vacuum to give of intermediates **1a** and **1b**, yields were 78% and 75%, respectively. Compound **2** was obtained by the reaction of 2-methylbenzo-[*d*]-thiazole (4 g, 15.6 mmol) with 1,3-dibromopropane (4 mL, 20 mmol). The reaction mixture was stirred at 100 °C for 24 h and cooled before suction filtration. The solid was washed with ethyl acetate, and vacuum dried to obtain a white solid, yield was 69%. The key intermediate compound **3a** or **3b** was then prepared by the reaction of **1a** (2 g, 6.2 mmol) or **1b** (1.89 g, 6.2 mmol) with **2** (2.17 g, 6.2 mmol) and potassium iodide (2.49 g, 15 mmol) in methanol (30 mL) respectively. The reaction mixture was stirred at 45 °C for 3 h. Ethyl acetate was added after the shock, filtered and washed with ethyl acetate before drying with vacuum to obtain red solid. Yields were recorded to be 90.1% and 88.6%, respectively.

4.3. General synthetic procedure for thiazole-quinolinium derivatives (4a1–4a4, 4b1–4b4, 4c1–4c2, 4d1–4d3 and 4e1–4e4)

The intermediate **3a** (0.2 mmol) or **3b** (0.2 mmol) was mixed with secondary amine (1.6 mmol) in 5 mL of DMSO. Then, the reaction mixture was stirred at 45 °C for 24 h, cooled and ethyl acetate was added after the shock, suction filtration, the solid was washed with ethyl acetate, and dried in vacuum to obtain compounds **4a1–4a4** and **4b1–4b4** in good yields. Then, **4a1–4a4** were subjected to a condensation reaction with *p*-methylthiobenzaldehyde, *p*-hydroxybenzaldehyde and indole-3-carbaldehyde in *n*-butanol the reaction mixture was stirred at 130 °C for 3 h. After cooled to room temperature, to the reaction mixture ethyl acetate was added to precipitate the solid products. The residuals were collected by suction filtration and dried in vacuum. The residuals were purified by silica column chromatography (dichloromethane: methanol (v : v), from 100 : 3 to 100 : 20) to obtain **4c1–4c2**, **4d1–4d3** and **4e1–4e4**. The characterizations of newly synthesized thiazole-quinolinium derivatives are as follow. For **4a2**, **4b1** and **4b2**, please refer to previous reports.[21]

4.3.1. (*Z*)-4-((3-(3-(Diethylamino)propyl)benzo[*d*]thiazol-2(3*H*)-ylidene)methyl)-1,2-dimethylquinolin-1-ium (4a1). Dark red solid, yield 83%; ^{1}H NMR (400 MHz, DMSO-d_6) δ 9.16 (s, 1H), 8.78 (d, J = 7.9 Hz, 1H), 8.24 (d, J = 8.8 Hz, 1H), 8.02 (dd, J = 14.6, 7.3 Hz, 2H), 7.80–7.72 (m, 2H), 7.63 (t, J = 7.5 Hz, 1H), 7.44 (dd, J = 14.6, 7.3 Hz, 2H), 6.87 (s, 1H), 4.67 (s, 2H), 4.15–4.05 (m, 3H), 3.18 (m, 4H), 2.94–2.85 (m, 3H), 2.13 (s, 3H), 1.20 (m, 6H). ^{13}C NMR (101 MHz, DMSO-d_6) δ 158.88, 155.04, 148.87, 140.36, 139.55, 133.73, 128.58, 126.98, 126.10, 124.83, 124.15, 123.99, 123.36, 118.88, 112.99, 112.71, 111.61, 86.90, 72.96, 63.56, 47.08, 40.03, 37.81, 23.38. HRMS *m*/*z*: calcd for $C_{26}H_{32}N_3S^+$ $[M - I]^+$ 418.23115; found 418.23118 $[M - I]^+$. Elemental analysis calculated for $C_{26}H_{32}N_3SI$, %: C 57.24, H 5.91, N 7.70. Found, %: C 57.11, H 6.06, N 7.62.

4.3.2. (*Z*)-1,2-Dimethyl-4-((3-(3-(piperidin-1-yl)propyl)benzo[*d*]thiazol-2(3*H*)-ylidene)methyl)quinolin-1-ium iodide (4a3). Dark red solid, yield 79%; ^{1}H NMR (400 MHz, DMSO-d_6) δ 8.68 (d, J = 8.3 Hz, 1H), 8.17 (d, J = 8.8 Hz, 1H), 8.08–7.90 (m, 2H), 7.75 (t, J = 8.1 Hz, 2H), 7.58 (t, J = 7.8 Hz, 1H), 7.38 (dd, J = 15.2, 7.6 Hz, 2H), 6.87 (s, 1H), 4.61 (t, J = 6.7 Hz, 2H), 4.06 (s, 3H), 2.87 (s, 3H), 2.34 (t, J = 6.7 Hz, 2H), 2.19 (m, 4H), 2.05–1.89 (m, 2H), 1.39–1.32 (m, 6H). ^{13}C NMR (101 MHz, DMSO-d_6) δ 159.22, 154.61, 148.47, 140.82, 139.57, 133.60, 128.40, 126.85, 125.62, 124.71, 124.22, 123.88, 123.17, 118.82, 113.32, 111.03, 87.02, 55.66, 54.57, 44.52, 40.00, 37.55, 25.96, 24.51, 24.16, 23.25. HRMS *m*/*z*: calcd for $C_{27}H_{32}N_3S^+$ $[M - I]^+$ 430.23115; found 430.23285 $[M - I]^+$. Elemental analysis calculated for $C_{27}H_{32}N_3SI$, %: C 58.17, H 5.79, N 7.54. Found, %: C 58.01, H 5.92, N 7.42.

4.3.3. (*Z*)-1,2-Dimethyl-4-((3-(3-(4-methylpiperidin-1-yl)propyl)benzo[*d*]thiazol-2(3*H*)-ylidene)methyl)quinolin-1-ium iodide (4a4). Dark red solid, yield 76%; ^{1}H NMR (400 MHz, DMSO-d_6) δ 8.67 (d, J = 8.3 Hz, 1H), 8.18 (d, J = 8.7 Hz, 1H), 8.00 (t, J = 7.7 Hz, 2H), 7.75 (t, J = 7.6 Hz, 2H), 7.59 (t, J = 7.8 Hz, 1H), 7.40 (t, J = 7.6 Hz, 1H), 7.34 (s, 1H), 6.87 (s, 1H), 4.60 (t, J = 6.5 Hz, 2H), 4.07 (s, 3H), 2.88 (s, 3H), 2.70 (m, 2H), 2.36 (s, 2H), 2.07–1.92 (m, 2H), 1.79 (m, 2H), 1.49 (m, 2H), 1.23 (s, 1H), 1.00 (m, 2H), 0.84 (d, J = 6.5 Hz, 3H). ^{13}C NMR (101 MHz, DMSO-d_6) δ 159.14, 154.54, 148.40, 140.75, 139.53, 133.56, 128.38, 126.85, 125.64, 124.68, 124.21, 123.86, 123.15, 118.80, 113.30, 111.01, 87.04, 55.19, 53.91, 44.42, 37.56, 34.32, 30.76, 24.27, 23.28, 22.26. HRMS *m*/*z*: calcd for $C_{28}H_{34}N_3S^+$ $[M - I]^+$ 444.24680; found 444.24708 $[M - I]^+$. Elemental analysis calculated for $C_{28}H_{34}N_3SI$, %: C 58.84, H 6.00, N 7.35. Found, %: C 58.71, H 6.15, N 7.22.

4.3.4. (*Z*)-1-Methyl-4-((3-(3-(piperidin-1-yl)propyl)benzo[*d*]thiazol-2(3*H*)-ylidene)methyl)quinolin-1-ium iodide (4b3). Red solid, yield 84%; ^{1}H NMR (400 MHz, DMSO-d_6) δ 8.86 (s, 1H), 8.70 (s, 1H), 8.07 (s, 3H), 7.82 (s, 2H), 7.64 (s, 1H), 7.44 (s, 2H), 6.94 (s, 1H), 4.71 (s, 2H), 4.22 (s, 3H), 4.13–4.00 (m, 1H), 3.17 (s, 3H), 2.89 (m, 2H), 2.23 (m, 2H), 1.64 (m, 6H). ^{13}C NMR (101 MHz, DMSO-d_6) δ 159.70, 149.48, 145.74, 140.37, 138.51, 133.81, 128.66, 127.59, 126.22, 125.02, 124.54, 124.30, 123.48, 118.86, 113.27, 108.73, 99.97, 87.87, 49.07, 43.06, 23.16. HRMS *m*/*z*: calcd for $C_{26}H_{30}N_3S^+$ $[M - I]^+$ 416.21550; found 416.21666 $[M - I]^+$. Elemental analysis calculated for $C_{26}H_{30}N_3SI$, %: C 57.46, H 5.56, N 7.73. Found, %: C 57.31, H 5.69, N 7.60.

4.3.5. (*Z*)-1-Methyl-4-((3-(3-(4-methylpiperidin-1-yl)propyl)benzo[*d*]thiazol-2(3*H*)-ylidene)methyl)quinolin-1-ium iodide (4b4). Red solid, yield 86%; ^{1}H NMR (400 MHz, DMSO-d_6) δ 8.86 (d, J = 8.4 Hz, 1H), 8.72 (t, J = 11.7 Hz, 1H), 8.08 (dt, J = 16.8, 8.4 Hz, 3H), 7.87–7.78 (m, 2H), 7.64 (t, J = 7.7 Hz, 1H), 7.44 (t, J = 8.0 Hz, 2H), 6.93 (s, 1H), 4.72 (s, 2H), 4.21 (d, J = 13.5 Hz, 3H), 3.03–2.77 (m, 3H), 2.24 (s, 2H), 1.77 (m, 3H), 1.63 (s, 2H), 1.33–1.24 (m, 2H), 0.91 (m, 4H). ^{13}C NMR (101 MHz, DMSO-d_6)

δ 159.60, 149.52, 145.69, 140.22, 138.43, 133.88, 128.73, 127.68, 126.14, 125.06, 124.50, 124.22, 123.42, 118.76, 113.13, 108.84, 87.74, 53.41, 52.66, 43.79, 43.09, 31.38, 30.67, 28.47, 28.34, 21.74, 21.44. HRMS *m*/*z*: calcd for $C_{27}H_{32}N_3S^+$ $[M - I]^+$ 430.23115; found 430.23263 $[M - I]^+$. Elemental analysis calculated for $C_{27}H_{32}N_3SI$, %: C 58.17, H 5.79, N 7.54. Found, %: C 58.05, H 5.89, N 7.45.

4.3.6. 2-((*E*)-2-(1*H*-Indol-3-yl)vinyl)-1-methyl-4-((*Z*)-(3-(3-morpholinopropyl)benzo[*d*]thiazol-2(3*H*)-ylidene)methyl) quinolin-1-ium iodide (4c1). Dark brown solid, yield 61%; ^{1}H NMR (400 MHz, DMSO-d_6) δ 8.65 (d, J = 8.3 Hz, 1H), 8.26 (s, 1H), 8.18 (t, J = 8.2 Hz, 2H), 8.05 (d, J = 7.6 Hz, 2H), 7.99 (d, J = 11.5 Hz, 2H), 7.78–7.70 (m, 3H), 7.57 (t, J = 7.8 Hz, 2H), 7.47 (m, 1H), 7.36 (m, 1H), 7.27 (d, J = 7.6 Hz, 2H), 6.88 (s, 1H), 4.62 (t, J = 6.3 Hz, 2H), 4.21 (s, 3H), 3.50 (s, 4H), 2.44–2.39 (m, 2H), 2.27 (s, 4H), 2.05–1.99 (m, 2H). ^{13}C NMR (101 MHz, DMSO-d_6) δ 157.70, 153.52, 147.22, 140.47, 139.36, 137.92, 136.98, 133.50, 133.26, 125.25, 125.13, 124.14, 123.99, 123.72, 123.41, 123.35, 121.71, 120.71, 114.01, 113.03, 107.66, 86.85, 66.68, 57.58, 53.68, 45.57, 38.21, 35.15, 24.56, 23.02, 19.11, 14.56, 14.33. HRMS *m*/*z*: calcd for $C_{35}H_{35}N_4OS^+$ $[M - I]^+$ 559.2526; found 559.2586 $[M - I]^+$. Elemental analysis calculated for $C_{35}H_{35}N_4OSI$, %: C 61.22, H 5.14, N 8.16. Found, %: C 61.09, H 5.26, N 8.05.

4.3.7. 2-((*E*)-4-Hydroxystyryl)-1-methyl-4-((*Z*)-(3-(3-morpholinopropyl)benzo[*d*]thiazol-2(3*H*)-ylidene)methyl)quinolin-1-ium iodide (4c2). Dark brown solid, yield 62%; ^{1}H NMR (400 MHz, DMSO-d_6) δ 8.28 (s, 1H), 7.85 (s, 2H), 7.77 (s, 1H), 7.51 (m, 6H), 7.20 (s, 1H), 6.74 (d, J = 14.6 Hz, 1H), 6.46 (s, 1H), 6.29 (d, J = 8.6 Hz, 2H), 4.33 (s, 2H), 3.89 (s, 3H), 3.59 (s, 6H), 2.34 (s, 2H), 2.26 (s, 3H), 1.88 (s, 2H), 1.37–0.74 (m, 1H). ^{13}C NMR (101 MHz, DMSO-d_6) δ 177.59, 154.76, 153.20, 145.05, 144.41, 141.16, 139.98, 132.55, 127.89, 125.32, 124.89, 123.57, 123.48, 123.28, 123.08, 121.25, 118.55, 118.12, 111.76, 108.05, 85.71, 66.59, 55.38, 53.83, 43.57, 37.19, 23.43. ESI-MS *m*/*z*: calcd for $C_{33}H_{34}N_3O_2S^+$ $[M - I]^+$ 536.24; found 536.25 $[M - I]^+$. Elemental analysis calculated for $C_{33}H_{34}N_3O_2SI$, %: C 59.73, H 5.16, N 6.33. Found, %: C 59.61, H 5.28, N 6.25.

4.3.8. 2-((*E*)-2-(1*H*-Indol-3-yl)vinyl)-1-methyl-4-((*Z*)-(3-(3-(pyrrolidin-1-yl)propyl)benzo[*d*]thiazol-2(3*H*)-ylidene)methyl) quinolin-1-ium iodide (4d1). Dark brown solid, yield 64%; ^{1}H NMR (400 MHz, DMSO-d_6) δ 8.24 (m, 2H), 8.04 (d, J = 7.9 Hz, 1H), 8.00–7.92 (m, 2H), 7.75 (m, 2H), 7.51 (m, 5H), 7.18 (m, 5H), 4.43 (t, J = 6.4 Hz, 2H), 3.99 (s, 3H), 2.43 (s, 6H), 1.98 (m, 2H), 1.70 (m, 4H). ^{13}C NMR (101 MHz, DMSO-d_6) δ 158.28, 153.91, 147.59, 140.83, 139.64, 137.95, 137.03, 133.20, 128.38, 126.51, 125.23, 124.11, 123.37, 121.70, 120.75, 114.51, 114.07, 113.06, 112.78, 107.95, 87.18, 53.92, 52.49, 38.30, 23.65. HRMS *m*/*z*: calcd for $C_{35}H_{35}N_4S^+$ $[M - I]^+$ 543.2582; found 543.2574 $[M - I]^+$. Elemental analysis calculated for $C_{35}H_{35}N_4SI$, %: C 62.68, H 5.26, N 8.35. Found, %: C 62.57, H 5.36, N 8.25.

4.3.9. 2-((*E*)-4-Hydroxystyryl)-1-methyl-4-((*Z*)-(3-(3-(pyrrolidin-1-yl)propyl)benzo[*d*]thiazol-2(3*H*)-ylidene)methyl)quinolin-1-ium iodide (4d2). Dark brown solid, yield 64%; ^{1}H NMR (400 MHz, DMSO-d_6) δ 8.57 (d, J = 8.4 Hz, 1H), 8.12 (d, J = 8.8 Hz, 1H), 8.03 (d, J = 7.8 Hz, 1H), 7.95 (d, J = 7.6 Hz, 1H), 7.76 (d, J = 8.5 Hz, 2H), 7.74–7.66 (m, 2H), 7.57 (m, 3H), 7.46 (d, J = 15.7 Hz, 1H), 7.36 (t, J = 7.6 Hz, 1H), 6.95 (s, 1H), 6.86 (d, J = 8.5 Hz, 2H), 4.59 (s, 2H), 4.12 (s, 3H), 2.49–2.43 (m, 2H), 2.38 (s, 4H), 1.99 (m, 2H), 1.67 (s, 4H). ^{13}C NMR (101 MHz, DMSO-d_6) δ 158.09, 153.85, 147.53, 140.92, 139.58, 137.96, 137.02, 133.43, 133.28, 128.28, 126.63, 125.40, 125.20, 124.24, 123.99, 123.87, 123.40, 121.73, 120.76, 118.98, 87.11, 66.53, 55.34, 53.78, 44.12, 38.30, 23.64. HRMS *m*/*z*: calcd for $C_{33}H_{34}N_3OS^+$ $[M - I]^+$ 520.2423; found 520.2424 $[M - I]^+$. Elemental analysis calculated for $C_{33}H_{34}N_3OSI$, %: C 61.20, H 5.29, N 6.49. Found, %: C 61.11, H 5.42, N 6.44.

4.3.10. 1-Methyl-2-((*E*)-4-(methylthio)styryl)-4-((*Z*)-(3-(3-(pyrrolidin-1-yl)propyl)benzo[*d*]thiazol-2(3*H*)-ylidene)methyl) quinolin-1-ium iodide (4d3). Dark brown solid, yield 58%; ^{1}H NMR (400 MHz, DMSO-d_6) δ 8.61 (s, 1H), 8.16 (s, 1H), 8.06 (s, 1H), 8.01–7.96 (m, 1H), 7.89 (d, J = 8.3 Hz, 2H), 7.74 (m, 3H), 7.66–7.58 (m, 3H), 7.39 (m, 3H), 7.02 (s, 1H), 4.64 (t, J = 6.3 Hz, 2H), 4.14 (s, 3H), 2.56 (m, 3H), 2.46 (m, 2H), 2.38 (m, 4H), 1.99 (m, 2H), 1.75–1.49 (m, 4H). ^{13}C NMR (101 MHz, DMSO-d_6) δ 158.09, 153.72, 147.31, 140.92, 139.58, 137.96, 137.02, 133.28, 125.20, 123.99, 121.73, 120.76, 118.98, 114.06, 107.80, 87.03, 66.62, 53.51, 38.30, 23.54. ESI-MS *m*/*z*: calcd for $C_{34}H_{36}N_3S_2^+$ $[M - I]^+$ 550.23; found 550.25 $[M - I]^+$. Elemental analysis calculated for $C_{34}H_{36}N_3S_2I$, %: C 60.26, H 5.35, N 6.20. Found, %: C 60.15, H 5.43, N 6.08.

4.3.11. 2-((*E*)-2-(1*H*-ndol-3-yl)vinyl)-1-methyl-4-((*Z*)-(3-(3-(piperidin-1-yl)propyl)benzo[*d*]thiazol-2(3*H*)-ylidene)methyl) quinolin-1-ium iodide (4e1). Dark brown solid, yield 71%; ^{1}H NMR (400 MHz, DMSO-d_6) δ 8.50 (d, J = 8.2 Hz, 1H), 8.21 (s, 1H), 8.07 (d, J = 8.6 Hz, 2H), 7.97 (m, 2H), 7.94–7.87 (m, 1H), 7.71 (s, 1H), 7.66–7.59 (m, 2H), 7.53 (m, 2H), 7.33–7.28 (m, 1H), 7.23 (m, 3H), 6.73 (s, 1H), 4.49 (t, J = 6.3 Hz, 2H), 4.11 (s, 3H), 2.77–2.66 (m, 2H), 2.35 (m, 2H), 1.99–1.91 (m, 3H), 1.83–1.75 (m, 2H), 1.54–1.46 (m, 2H), 1.18 (m, 1H), 1.05 (m, 1H), 0.84 (m, 3H). ^{13}C NMR (101 MHz, DMSO-d_6) δ 185.42, 153.77, 147.00, 141.01, 139.69, 137.22, 133.25, 128.16, 126.33, 125.63, 124.01, 123.84, 123.39, 123.24, 122.52, 121.66, 121.23, 120.72, 114.61, 113.70, 113.00, 107.87, 86.90, 55.22, 53.95, 38.11, 34.39, 30.81, 24.19, 22.29, 19.02. HRMS *m*/*z*: calcd for $C_{37}H_{39}N_4S^+$ $[M - I]^+$ 571.2890; found 571.2933 $[M - I]^+$. Elemental analysis calculated for $C_{37}H_{39}N_4SI$, %: C 63.60, H 5.63, N 8.02. Found, %: C 63.50, H 5.75, N 7.91.

4.3.12. 2-((*E*)-4-Hydroxystyryl)-1-methyl-4-((*Z*)-(3-(3-(piperidin-1-yl)propyl)benzo[*d*]thiazol-2(3*H*)-ylidene)methyl) quinolin-1-ium iodide (4e2). Dark brown solid, yield 59%; ^{1}H NMR (400 MHz, DMSO-d_6) δ 8.72 (s, 1H), 8.16 (d, J = 8.7 Hz, 1H), 8.06–7.94 (m, 2H), 7.82–7.73 (m, 4H), 7.67–7.49 (m, 4H), 7.38 (t, J = 7.5 Hz, 1H), 6.97–6.81 (m, 3H), 4.62 (m, 2H), 4.15 (m, 3H), 2.09 (m, 3H), 1.62 (m, 4H), 1.22 (m, 4H), 0.86 (m, 6H). ^{13}C NMR (101 MHz, DMSO-d_6) δ 187.85, 175.91, 144.21, 141.09, 139.83, 132.92, 132.67, 128.10, 123.85, 123.73, 121.29, 119.37, 119.16, 112.36, 110.20, 108.06, 86.52, 55.25, 53.96, 37.77, 34.40, 30.82, 24.10, 22.29. HRMS *m*/*z*: calcd for $C_{35}H_{38}N_3OS^+$ $[M - I]^+$ 548.2730; found 548.2749 $[M - I]^+$. Elemental analysis calculated for $C_{35}H_{38}N_3OSI$, %: C 62.22, H 5.67, N 6.22. Found, %: C 62.10, H 5.74, N 6.11.

4.3.13. 1-Methyl-2-((*E*)-4-(methylthio)styryl)-4-((*Z*)-(3-(3-(piperidin-1-yl)propyl)benzo[*d*]thiazol-2(3*H*)-ylidene)methyl)

quinolin-1-ium iodide (4e3). Dark brown solid, yield 65%; ^{1}H NMR (400 MHz, DMSO-d_6) δ ^{1}H NMR (400 MHz, DMSO) δ 8.72 (s, 1H), 8.10 (m, 2H), 7.99–7.94 (m, 1H), 7.89 (d, J = 8.1 Hz, 2H), 7.77–7.68 (m, 3H), 7.59 (m, 3H), 7.48–7.28 (m, 3H), 6.86 (s, 1H), 4.62 (m, 2H), 4.13 (s, 3H), 3.02 (m, 4H), 2.09 (m, 3H), 1.61 (m, 2H), 1.45 (m, 2H), 1.22 (m, 4H), 0.87 (m, 4H). ^{13}C NMR (101 MHz, DMSO-d_6) δ 159.82, 154.69, 147.72, 141.02, 139.68, 137.11, 133.22, 130.61, 124.72, 124.27, 124.02, 123.37, 121.70, 114.07, 108.03, 104.24, 90.18, 89.40, 87.20, 66.53, 55.38, 53.79, 38.33, 23.66. HRMS m/z: calcd for $C_{36}H_{40}N_3S_2^+$ [M − I]$^+$ 578.2658; found 578.2687 [M − I]$^+$. Elemental analysis calculated for $C_{36}H_{40}N_3S_2I$, %: C 61.27, H 5.71, N 5.95. Found, %: C 61.14, H 5.84, N 5.87.

4.3.14. 2-((*E*)-4-(Dimethylamino)styryl)-1-methyl-4-((*Z*)-(3-(3-(piperidin-1-yl)propyl)benzo[*d*]thiazol-2(3*H*)-ylidene)methyl) quinolin-1-ium iodide (4e4). Dark brown solid, yield 57%; ^{1}H NMR (400 MHz, DMSO-d_6) δ 8.60 (d, J = 8.3 Hz, 1H), 8.14–7.93 (m, 3H), 7.81 (d, J = 8.6 Hz, 2H), 7.72–7.66 (m, 3H), 7.62 (s, 1H), 7.58–7.36 (d, J = 7.6 Hz, 3H), 6.86–6.77 (m, 3H), 4.58 (t, J = 5.7 Hz, 2H), 4.14 (s, 3H), 3.04 (s, 6H), 2.72 (m, 2H), 2.36 (m, 2H), 2.01–1.94 (m, 2H), 1.78 (m, 2H), 1.49 (m, 2H), 1.07–0.98 (m, 2H), 0.83 (m, 4H). ^{13}C NMR (101 MHz, DMSO-d_6) δ 165.93, 158.40, 156.93, 153.18, 152.30, 140.95, 139.63, 131.01, 124.15, 123.90, 123.44, 123.18, 120.38, 119.02, 115.19, 112.92, 112.18, 111.51, 108.03, 55.24, 53.95, 38.34, 34.39, 30.80, 22.30. HRMS m/z: calcd for $C_{37}H_{43}N_4S^+$ [M − I]$^+$ 575.3203; found 575.3230 [M − I]$^+$. Elemental analysis calculated for $C_{37}H_{43}N_4SI$, %: C 63.24, H 6.17, N 7.97. Found, %: C 63.18, H 6.23, N 7.88.

4.4. MIC and MBC assays

MIC tests were conducted using high throughput 96-well microtiter plates method with clinically relevant bacterial strains – (a) Gram-positive: *S. aureus* ATCC 29213, *S. aureus* ATCC 43300, *S. aureus* ATCC BAA-41, *S. aureus* ATCC BAA-44, *S. aureus* ATCC BAA-1747, *S. aureus* ATCC BAA-1720, *E. faecalis* ATCC 29212, *E. faecium* ATCC 49624, *E. faecium* ATCC 700221, *S. epidermidis* ATCC 12228, *B. subtilis* 168; (b) Gram-negative: *E. coli* ATCC 25922, *E. coli* ATCC 8739, *E. coli* ATCC BAA-2469, *K. pneumoniae* ATCC BAA-2470, *A. baumannii* ATCC 19606, *P. aeruginosa* ATCC BAA-2108, *E. cloacae* ATCC BAA-1143. The overnight culture was diluted in Mueller–Hinton broth medium to a final concentration of 5×10^5 CFU mL^{-1}, compounds were serially diluted with DMSO and then added into microtiter plates containing the test bacteria with a final DMSO concentration of 1%. After 18–24 h incubation at 37 °C, the minimum drug concentration without bacterial growth was determined as the MIC value. The MIC was defined as the lowest compound concentration at which 90% of bacteria growth was inhibited. Methicillin, ampicillin, vancomycin and rifampin were applied as a reference compound under the same assay conditions. For the minimal bactericidal concentration (MBC) assays, 100 μL of medium from the MIC microtiter plates assay with no visible turbidity was spread on freshly prepared MH agar plates and incubated at 37 °C for 24 h before colony counting. The MBC of the derivatives was described as the lowest concentration of the derivative with less than five colonies grow on each plate.[36] Then, the MBC/MIC ratios were calculated, a compound was considered as bactericidal when the MBC/MIC ratio was ≤4 and bacteriostatic when the MBC/MIC ratio was >4.[22,23] Each assay was carried out in triplicates.

4.5. Bacterial morphology studies

The *B. subtilis* strain 168 cells were grown in LB medium. Bacterial culture was prepared at concentration of 1×10^5 CFU mL^{-1} and inoculated in the same medium containing the test compound at a concentration of 0.5 × MIC. After incubated at 37 °C for 4 h, the cell pellet was collected before resuspension in PBS. 3 μL of the suspension mixture was then loaded on a microscopic slide precoated with 0.1% (w/v) poly-L-lysine and the morphology of the bacterial cells was visualized under a high resolution laser confocal microscope at 40× oil immersion magnification. The images were captured using a ZEISS LSM 800 with Airscan microscope.

4.6. Membrane integrity studies

B. subtilis 168 cells were grown in LB medium. The bacterial culture was then diluted to 1×10^5 CFU mL^{-1} and inoculated in the same medium added with the test compound at a concentration of 0.5 × MIC. After incubation period of 4 h at 37 °C, 1.6 μM of FM 4–64 (a fluorescent dye) was added into the medium and further incubated for an additional 15 min at 37 °C without shaking. The cells were then collected *via* centrifugation and resuspended in PBS. Then, 3 μL of PBS containing bacterial cells was placed on the microscopy slide precoated with 0.1% (w/v) poly-L-lysine. Changes in morphology of the bacterial cells were monitored under a high resolution laser confocal microscope at 40× oil immersion magnification. The images were captured using a ZEISS LSM 800 with Airscan microscope.

4.7. Light-scattering assay

As the polymer mass of FtsZ correlates directly to the magnitude of light scattering signal, the dynamics of FtsZ assembly can be studied *in vitro*.[37] The polymerization of *S. aureus* FtsZ was monitored by 90° light scattering in a PerkinElmer LS-45 fluorescence spectrometer. Both excitation and emission wavelengths were set at 600 nm with a slit width of 2.5 nm.[38] *S. aureus* FtsZ (4 μM) in 50 mM MOPS buffer (pH 6.5) was incubated with vehicle control (1% DMSO) or varied concentrations of the tested compound for 10 min at 25 °C. Subsequently, baseline was established with 50 mM KCl and 10 mM $MgCl_2$. Ten minutes after the baseline establishment, 1 mM GTP was added at the last fraction and the increase in light scattering was measured for another 25 minutes. The rate and extent of polymerization were calculated with subtraction of background using appropriate blank. Each assay was carried out in triplicates.

4.8. *Sa*FtsZ binding affinity assay

Fluorescence spectroscopy is the most rapid and direct means of detecting protein and small molecule interactions. The binding of **4a4** and **4b4** to *Sa*FtsZ was determined by monitoring

changes in protein-induced intrinsic fluorescence of the compounds. An aliquot of the *Sa*FtsZ stock solution was sequentially added to a buffer solution (600 μL) containing **4a4** (3.51 μM) or **4b4** (3.68 μM) to increase the protein concentration by a gradient of 0.4 μM. After each addition of the protein, the reaction was equilibrated for 2 minutes and then the emission spectra were obtained from 700 nm to 500 nm in 1 nm increments. Subtract the background spectrum produced by protein titration into a separate buffer. Fluorescence spectra were recorded on a PerkinElmer LS-45 fluorescence spectrometer with an excitation wavelength set at 493 nm and a buffer condition of 50 mM Tris–HCl (pH 7.4), 50 mM KCl and 2 mM magnesium acetate. All measurements were taken at 25 °C.

4.9. GTPase activity assay

The GTPase activity of *S. aureus* FtsZ was determined using a ATPase/GTPase Activity Assay Kit (Sigma-Aldrich, USA) according the manufacturer's instructions with minor modifications.[27] *S. aureus* FtsZ (7.3 μM) was added to assay buffer with vehicle (1% DMSO) or varied concentrations of test compound. Reactions were initiated by the addition of 200 μM GTP and incubated at room temperature. After 30 min of incubation, 200 μL of reagent was added into each well and incubated for another 30 minutes at room temperature to halt the enzymatic reaction and generate the colorimetric product. Inorganic phosphate was quantified spectrometrically at 620 nm with a microplate reader. Each assay was carried out in triplicates.

4.10. Visualization of Z-ring in bacterial cells

B. subtilis containing the IPTG-inducible plasmid for the production of green fluorescent protein (GFP)-tagged FtsZ was included in the current study to facilitate visualization of Z-ring. A culture of *B. subtilis* was grown in LB medium (supplemented with 30 μg mL^{-1} of chloramphenicol) at 37 °C in shaking incubator. Overnight grown cultures were diluted to 1% with LB medium containing 40 μM of IPTG and selected test compound at a concentration of 0.5 × MIC. After 4 h incubation at 37 °C, *B. subtilis* cells were fixed, harvested and resuspended in PBS buffer. 3 μL of sample mixtures were added to the pretreated microscopy slide with 0.1% (w/v) poly-L-lysine and visualized using a high resolution laser confocal microscope at 40× oil immersion magnification. The images were captured using a ZEISS LSM 800 with Airscan microscope.

4.11. CCK-8 cytotoxicity assay

The cytotoxicity of compounds was explored with human bronchial epithelium cells (16HBE), human renal tubular epithelial cells (HK-2) and mouse fibroblast cells (L929) by CCK-8 (Cell Counting Kit-8) method. For the cytotoxicity assay, 5000 cells were seeded per well in a 96-wells microtiter plate and allowed to adhere overnight at 37 °C before treatment with selected compound. After 48 h of treatment with selected compounds, 10 μL CCK-8 was added to each well and incubated for another 3 h, then the absorbance were measured at 450 nm with a microplate reader. Each assay was carried out in triplicates.

4.12. Hemolytic activity assay

Compounds were tested with human erythrocytes at a concentration of 2% as previously described.[32] Serial dilution of selected compounds was prepared in PBS and then 150 μL was loaded per well in a 96-well microtiter plate before addition of 150 μL of human blood. After incubated 1 h at 37 °C, plates were centrifuged at 10 000 rpm for 5 min, then 100 μL of the supernatant was used to obtain absorbance reading at 540 nm. Water and PBS were used as positive and negative control respectively. The hemolysis percentage was calculated with the equation (absorbance of test compound − absorbance of the negative control)/(absorbance of water − absorbance of the negative control) × 100%, and a rate > 5% indicates hemolysis.[39] Each assay was carried out in triplicates.

4.13. *In vitro* evaluation of potential drug resistance development

To further evaluate potential development of drug resistance induced these compounds and antibiotics (ciprofloxacin, vancomycin, rifampin) against bacterial strains (*S. aureus* ATCC 29213, *B. subtilis* 168, *E. coli* ATCC 25922), we refer to reported methods for drug resistance studies.[34,40] The bacterial culture at a concentration of 0.5 × MIC in a 96-well microtiter plate of the initial MIC test was diluted to 5 × 10^5 CFU mL^{-1}, and then various concentrations of compounds were added to the corresponding bacteria, the MICs were determined after incubated 24 h at 37 °C. This process was repeated for 35 times.

4.14. Molecular docking study

Molecular modeling procedures were carried out using Discovery Studio (DS) version 2016 X-ray crystal structure of *Sa*FtsZ downloaded from the PDB database (PDB code: 4DXD). The ligands were sketched using the tools of small molecules in DS. After removing water molecules and co-crystal ligands, the protein was subjected for docking using an automated procedure of DS-LibDock protocol.

Conflicts of interest

There are no conflicts to declare.

Acknowledgements

We acknowledge the support from the National Natural Science Foundation of China (81703333, 81670480 and 81473082), Natural Science Foundation of Guangdong Province, China (2020A1515011326, 2017A030313078), Guangzhou Key Laboratory Fund (201905010004), and Major Scientific Research Projects at Provincial Level in Guangdong General University (2017KZDXM068). The authors are also grateful to the support from Department of Agriculture and Rural Affairs of Guangdong Province, China (2018LM2175), and Science and Technology Program of Guangzhou Municipal Health Commission (20192A011018).

References

1 K. K. Kumarasamy, M. A. Toleman, T. R. Walsh, J. Bagaria, F. Butt, R. Balakrishnan, U. Chaudhary, M. Doumith, C. G. Giske, S. Irfan, P. Krishnan, A. V. Kumar, S. Maharjan, S. Mushtaq, T. Noorie, D. L. Paterson, A. Pearson, C. Perry, R. Pike, B. Rao, U. Ray, J. B. Sarma, M. Sharma, E. Sheridan, M. A. Thirunarayan, J. Turton, S. Upadhyay, M. Warner, W. Welfare, D. M. Livermore and N. Woodford, *Lancet Infect. Dis.*, 2010, **10**, 597–602.

2 T. R. Walsh, J. Weeks, D. M. Livermore and M. A. Toleman, *Lancet Infect. Dis.*, 2011, **11**, 355–362.

3 D. J. Payne, *Science*, 2008, **321**, 1644–1645.

4 N. Sun, Y. J. Lu, F. Y. Chan, R. L. Du, Y. Y. Zheng, K. Zhang, L. Y. So, R. Abagyan, C. Zhuo, Y. C. Leung and K. Y. Wong, *Front. Microbiol.*, 2017, **8**, 855.

5 G. D. Wright, *Chem. Biol.*, 2012, **19**, 3–10.

6 D. N. Margalit, L. Romberg, R. B. Mets, A. M. Hebert, T. J. Mitchison, M. W. Kirschner and D. RayChaudhuri, *Proc. Natl. Acad. Sci. U. S. A.*, 2004, **101**, 11821–11826.

7 Q. Huang, F. Kirikae, T. Kirikae, A. Pepe, A. Amin, L. Respicio, R. A. Slayden, P. J. Tonge and I. Ojima, *J. Med. Chem.*, 2006, **49**, 463–466.

8 P. Sass and H. Brotz-Oesterhelt, *Curr. Opin. Microbiol.*, 2013, **16**, 522–530.

9 P. Domadia, S. Swarup, A. Bhunia, J. Sivaraman and D. Dasgupta, *Biochem. Pharmacol.*, 2007, **74**, 831–840.

10 P. N. Domadia, A. Bhunia, J. Sivaraman, S. Swarup and D. Dasgupta, *Biochemistry*, 2008, **47**, 3225–3234.

11 D. J. Haydon, N. R. Stokes, R. Ure, G. Galbraith, J. M. Bennett, D. R. Brown, P. J. Baker, V. V. Barynin, D. W. Rice, S. E. Sedelnikova, J. R. Heal, J. M. Sheridan, S. T. Aiwale, P. K. Chauhan, A. Srivastava, A. Taneja, I. Collins, J. Errington and L. G. Czaplewski, *Science*, 2008, **321**, 1673–1675.

12 M. Kaul, L. Mark, Y. Zhang, A. K. Parhi, Y. L. Lyu, J. Pawlak, S. Saravolatz, L. D. Saravolatz, M. P. Weinstein, E. J. LaVoie and D. S. Pilch, *J. Antimicrob. Chemother.*, 2015, **59**, 4845–4855.

13 E. L. White, W. J. Suling, L. J. Ross, L. E. Seitz and R. C. Reynolds, *J. Antimicrob. Chemother.*, 2002, **50**, 111–114.

14 N. Sun, F. Y. Chan, Y. J. Lu, M. A. Neves, H. K. Lui, Y. Wang, K. Y. Chow, K. F. Chan, S. C. Yan, Y. C. Leung, R. Abagyan, T. H. Chan and K. Y. Wong, *PLoS One*, 2014, **9**, e97514.

15 N. Sun, Y. Y. Zheng, R. L. Du, S. Y. Cai, K. Zhang, L. Y. So, K. C. Cheung, C. Zhuo, Y. J. Lu and K. Y. Wong, *Medchemcomm*, 2017, **8**, 1909–1913.

16 A. Janas and P. Przybylski, *Eur. J. Med. Chem.*, 2019, **182**, 111662.

17 S. Singh, G. Kaur, V. Mangla and M. K. Gupta, *J. Enzyme Inhib. Med. Chem.*, 2015, **30**, 492–504.

18 N. Sun, L. Ban, M. Li, Z. Y. Fang, X. M. Li, W. X. Yao, J. H. Pan, Y. J. Lu, Z. H. Liu and W. L. Wong, *J. Pharmacol. Sci.*, 2018, **138**, 83–85.

19 N. Sun, R. L. Du, Y. Y. Zheng, Q. Guo, S. Y. Cai, Z. H. Liu, Z. Y. Fang, W. C. Yuan, T. Liu, X. M. Li, Y. J. Lu and K. Y. Wong, *J. Enzyme Inhib. Med. Chem.*, 2018, **33**, 879–889.

20 Y. J. Lu, Q. Deng, J. Q. Hou, D. P. Hu, Z. Y. Wang, K. Zhang, L. G. Luyt, W. L. Wong and C. F. Chow, *ACS Chem. Biol.*, 2016, **11**, 1019–1029.

21 W. Long, Y. J. Lu, K. Zhang, X. H. Huang, J. Q. Hou, S. Y. Cai, Y. Li, X. Du, L. G. Luyt, W. L. Wong and C. F. Chow, *Dyes Pigm.*, 2018, **159**, 449–456.

22 J. Meletiadis, C. Antachopoulos, T. Stergiopoulou, S. Pournaras, E. Roilides and T. J. Walsh, *J. Antimicrob. Chemother.*, 2007, **51**, 3329–3337.

23 F. C. Bi, D. Song, N. Zhang, Z. Y. Liu, X. J. Gu, C. Y. Hu, X. K. Cai, H. Venter and S. T. Ma, *Eur. J. Med. Chem.*, 2018, **159**, 90–103.

24 J. M. Andreu, C. Schaffner-Barbero, S. Huecas, D. Alonso, M. L. Lopez-Rodriguez, L. B. Ruiz-Avila, R. Nunez-Ramirez, O. Llorca and A. J. Martin-Galiano, *J. Biol. Chem.*, 2010, **285**, 14239–14246.

25 M. Kaul, L. Mark, Y. Z. Zhang, A. K. Parhi, E. J. LaVoie and D. S. Pilch, *Biochem. Pharmacol.*, 2013, **86**, 1699–1707.

26 Y. Li, J. Hsin, L. Zhao, Y. Cheng, W. Shang, K. C. Huang, H.-W. Wang and S. Ye, *Science*, 2013, **341**, 392–394.

27 F. Y. Chan, N. Sun, M. A. Neves, P. C. Lam, W. H. Chung, L. K. Wong, H. Y. Chow, D. L. Ma, P. H. Chan, Y. C. Leung, T. H. Chan, R. Abagyan and K. Y. Wong, *J. Chem. Inf. Model.*, 2013, **53**, 2131–2140.

28 F. H. Stootman, D. M. Fisher, A. Rodger and J. R. Aldrich-Wright, *Analyst*, 2006, **131**, 1145–1151.

29 X. Xie, B. Choi, E. Largy, R. Guillot, A. Granzhan and M. P. Teulade-Fichou, *Chem.–Eur. J.*, 2013, **19**, 1214–1226.

30 T. K. Beuria, P. Singh, A. Surolia and D. Panda, *Biochem. J.*, 2009, **423**, 61–69.

31 T. K. Beuria, M. K. Santra and D. Panda, *Biochemistry*, 2005, **44**, 16584–16593.

32 Z. J. Zheng, N. Tharmalingam, Q. Z. Liu, E. Jayamani, W. Kim, B. B. Fuchs, R. J. Zhang, A. Vilcinskas and E. Mylonakis, *J. Antimicrob. Chemother.*, 2017, **61**, e00686-17.

33 D. J. Haydon, N. R. Stokes, R. Ure, G. Galbraith, J. M. Bennett, D. R. Brown, P. J. Baker, V. V. Barynin, D. W. Rice, S. E. Sedelnikova, J. R. Heal, J. M. Sheridan, S. T. Aiwale, P. K. Chauhan, A. Srivastava, A. Taneja, I. Collins, J. Errington and L. G. Czaplewski, *Science*, 2008, **321**, 1673–1675.

34 H. K. Lui, W. Gao, K. C. Cheung, W. B. Jin, N. Sun, J. W. Y. Kan, I. L. K. Wong, J. Chiou, D. Lin, E. W. C. Chan, Y.-C. Leung, T. H. Chan, S. Chen, K.-F. Chan and K.-Y. Wong, *Eur. J. Med. Chem.*, 2019, **163**, 95–115.

35 M. Kaul, Y. Z. Zhang, A. K. Parhi, E. J. LaVoie and D. S. Pilch, *Biochem. Pharmacol.*, 2014, **89**, 321–328.

36 Z. Q. Qin, J. Zhang, B. Xu, L. L. Chen, Y. Wu, X. M. Yang, X. Shen, S. Molin, A. Danchin, H. L. Jiang and D. Qu, *BMC Microbiol.*, 2006, **6**, 96.

37 A. Mukherjee and J. Lutkenhaus, *J. Bacteriol.*, 1999, **181**, 823–832.

38 Z. Y. Fang, L. Ban, Y. A. Li, W. C. Yuan, Z. H. Liu, T. Liu, X. M. Li, K. Y. Wong, Y. J. Lu, N. Sun and X. G. Yao, *J. Pharmacol. Sci.*, 2018, **137**, 283–289.

39 S. Lim, S. Lee, S. H. Yi, Y. S. Son, S. M. Choi and Y. K. Kim, *Evid.-Based Complementary Altern. Med.*, 2010, **7**, 259–264.

40 S. M. Lin, J. J. Koh, T. T. Aung, W. L. W. Sin, F. H. Lim, L. Wang, R. Lakshminarayanan, L. Zhou, D. T. H. Tan, D. R. Cao, R. W. Beuerman, L. Ren and S. P. Liu, *J. Med. Chem.*, 2017, **60**, 6152–6165.